EES Batteries

ROYAL SOCIETY OF CHEMISTRY

PAPER

View Article Online
View Journal | View Issue

Cite this: *EES Batteries*, 2025, **1**, 840

Multifunctional scavengers in an MOF-Al_2O_3-based Janus separator for high-voltage lithium batteries†

S. Davino,[a] P. Mustarelli,[b,c] D. Callegari *[a,b] and E. Quartarone[a,b]

$LiPF_6$-based electrolytes undergo degradation when exposed to even small humidity traces, generating HF that usually causes corrosion of Ni/Mn-based cathodes (*e.g.* $LiNi_{0.5}Mn_{1.5}O_4$ spinel, LNMO) with consequent loss of transition metal (TM) ions. This phenomenon leads to detrimental phenomena responsible for the significant reduction of both capacity and lifetime of Li-based batteries. Here, a multifunctional P(VDF-HFP)-based Janus separator for smart Li batteries is developed to prevent the above-mentioned degradation phenomena. The multi-functions consist of two different scavengers for HF and H_2O, respectively. Alumina nanoparticles are used as HF trapping agents, given their ability to react with hydrofluoric acid, while a metal–organic framework (HKUST-1) is chosen as a molecular sieve for the water molecules. The Janus membrane was tested as a separator in an LNMO half-cell under harsh conditions with a water-enriched (100 ppm) electrolyte. The Janus separator exhibits significantly enhanced cycling performance, with capacity retention exceeding 90% after 200 cycles at 1C (>120 mA h g^{-1}), in contrast to the bare P(VDF-HFP) film, showing capacity retention lower than 70%. Post-cycling ICP-OES analysis revealed that the leaching of TM metal ions from the spinel lattice upon cycling is halved in the case of cells with a Janus membrane as the separator. Moreover, the synergistic effects of the two scavengers (Al_2O_3 and an MOF) in the LNMO-based cells are remarkably beneficial in terms of enhanced resistance towards thermal runaway. The Janus separator, including scavenging functions, has great potential to enhance the quality, lifetime and safety of next-generation Li-based batteries.

Received 31st January 2025,
Accepted 13th May 2025

DOI: 10.1039/d5eb00017c

rsc.li/EESBatteries

Broader context

There are several mechanisms involved in the degradation of materials and components of Li ion and Li metal batteries, mainly related to the liquid electrolyte. $LiPF_6$-based systems, for example, undergo transition metal (TM) dissolution triggered by HF generation in consequence of salt decomposition catalysed by even small water traces. TM ions can cause anode crosstalk, thereby reducing the cell performances, especially cycling stability and safety. In this work, we present a multifunctional P(VDF-HFP)-based Janus separator for smart Li batteries, developed to prevent such detrimental phenomena. The separator is designed to assemble two thin layers: one containing a specific MOF (HKUST-1) and the other including alumina nanoparticles. The nanometric Al_2O_3 acts as a HF scavenger, thereby leading to an efficient TM ion-trapping layer, whilst HKUST-1 acts as a sieve to reversibly block water molecules in its channels. As a result, the use of a double-scavenger separator has been shown to effectively mitigate the dissolution of TMs and ion crosstalk. Furthermore, the synergistic effects of the two scavengers within the cells are significantly beneficial in terms of enhanced resistance towards thermal runaway, thereby improving their lifespan and safety.

1. Introduction

The increasing demand for electric mobility is driving the development of better lithium-ion batteries[1,2] employing new strategies (*e.g.* layers, coating, doping, internal sensing, additives, self-healing *etc.*) that aim at improving the cell quality, reliability, lifetime, and safety (QRLS).[3,4]

The most widely used electrolytes are based on $LiPF_6$ due to its excellent ionic conductivity and electrochemical stability. However, this salt undergoes autocatalytic decomposition at temperatures above 50 °C and in the presence of impurities,

[a]*Department of Chemistry, University of Pavia, Via Taramelli 12, Pavia 27100, Italy. E-mail: daniele.callegari@unipv.it*
[b]*GISEL Centro di Riferimento Nazionale per i Sistemi di Accumulo Elettrochimico di Energia, INSTM, Firenze 50121, Italy*
[c]*Dept. of Materials Science, University of Milano Bicocca, Via Cozzi 55, Milano 20125, Italy*

† Electronic supplementary information (ESI) available. See DOI: https://doi.org/10.1039/d5eb00017c

especially water,[5,6] generating detrimental by-products such as POF_x and HF, according to the following reaction:

$$LiPF_{6(s)} + H_2O_{(l)} \rightarrow LiF_{(s)} + POF_{3(g)} + 2HF_{(g)}$$

This reaction results in a harsh environment that accelerates cell degradation.[7] In particular, HF leaches the transition metal (TM) ions from the Ni–Mn-based cathodes (*e.g.*, spinel $LiNi_{0.5}Mn_{1.5}O_4$, LNMO, or layered NMC).[8] The dissolution of TMs from the active material causes several problems, including the following: (i) a decrease of reversible capacity, (ii) instability of the electrode–electrolyte interface, (iii) evolution of molecular oxygen or superoxide radicals from the lattice, (iv) chemical cross-talk through the electrolyte with consequent deposition of the metal ions onto the anode, and (v) reaction of TM ions with the SEI consuming Li^+ and forming a high resistance passivation layer that inhibits Li diffusion.[5,9,10] Moreover, the dissolution of TMs boosts the degradation of carbonate solvents by superoxide radicals ($O_2^{\bullet-}$), generating gaseous species (CO and CO_2) and water with a consequent increase in internal pressure.[11] All these phenomena drastically shorten the battery lifetime and cause severe safety concerns.

The design of scavengers of such detrimental small molecules (*e.g.* HF, H_2O, O_2, CO_2) is currently one of the most promising strategies in the development of next-generation smart lithium-ion batteries. The main goal is to mitigate stability issues, promoting longer cell lifetime and improving the functional performance, including safety. Scavengers have been recently investigated as dopants, buffering layers or coatings for the cathode, but also as active additives in the electrolyte. In the latter case, Lewis bases with electron-donating sites such as aminosilanes, silyl ethers, isocyanate moieties, and phosphites were used for their scavenging ability.[5,12,13]

To minimize any negative impact on the electrolyte properties, an alternative strategy is the incorporation of scavengers into the separator through filler dispersion or chemical functionalization. This approach allows for the easy processing of the polymers usually employed as separators.[14] In the literature, there are a few examples of scavenging separators for acid, water and transition metal trapping, usually consisting of inorganic ceramic particles having low cost, high temperature resistance, and the ability to enhance mechanical strength.[15,16] Several metal oxides, including Al_2O_3, CuO, SiO_2, ZnO, and ZrO_2, were specifically used as fillers in composite separators with demonstrated capability to capture HF through trapping reactions by forming metal fluoride, thereby hindering the acid release in the electrolyte.[17–20] Qiu *et al.*, for example, reported on a double-coating of the polyethylene separator with layers of a silica–oxygen–borate network and Al_2O_3 nanoparticles in a $LiN_{0.5}Mn_{0.3}Co_{0.2}O_2$|graphite cell, resulting in excellent thermal stability and combined HF/H_2O scavenging activity. The functionalized separator exhibited a capacity retention of 68% after 400 cycles.[21]

As an alternative to metal oxides, metal–organic frameworks (MOFs) were also used in the design of advanced materials for Li-ion cells as coatings,[22,23] fillers,[24,25] and electrolytes.[26–28] MOFs are porous materials based on a metal center coordinated to organic linkers.[29,30] Among the wide variety of proposed structures, HKUST-1 (MOF-199 or CuBTC) is one of the most interesting ones due to its active porous network.[31] This material has a 3D-channel structure connecting a system of cages formed by two octahedrally arranged Cu atoms, which are coordinated to the oxygen atoms of the carboxylate units of trimeric acid. The channels and cages allow for the sorption of water molecules onto the unsaturated metal sites, making it capable of scavenging water.[32] Chang *et al.* recently reported on a water scavenger separator based on HKUST-1 paired with a $LiNi_{0.8}Mn_{0.1}Co_{0.1}O_2$ cathode that could deliver a great suppression of transition metal loss and superior cycling stability with 72% capacity retention in a 200 ppm water-containing electrolyte.[33]

In this work, we further explore the potential of MOFs as efficient water scavengers for separators in LIBs when they are synergistically combined with nanosized metal oxides (MO_x). The strategy is to simultaneously capture detrimental small molecules (H_2O and HF) by coupling the trapping capability of scavengers, which are usually highly selective towards one single specific species (namely MOF and MO_x for H_2O and HF, respectively). More specifically, a P(VDF-HFP) Janus separator has been properly designed, assembling two thin layers, one containing HKUST-1 as a water trapping unit and the second one including Al_2O_3 nanoparticles as acid scavengers. A Janus membrane benefits modulable functions while maintaining high amounts of additives in the polymer matrix without worsening the intrinsic polymer flexibility. Moreover, recent literature on such engineered multifunctional membranes has demonstrated significant improvement in the battery cell performance when they are used as separators in place of Celgard™-based systems.[34–36]

The scavenging Janus separator was investigated from thermal, mechanical, and morphological points of view to understand the role played by both the fillers in improving the electrochemical properties. The functional performances were evaluated in LNMO-based cells with a water-enriched $LiPF_6$-based liquid electrolyte. ICP *post-mortem* analyses were specifically carried out to evaluate the TM dissolution rate. Accelerated rate calorimetry (ARC) analysis was finally performed to demonstrate the robustness of the Janus separator, also in terms of cell thermal stability. Our results demonstrate that these novel functionalized separators are promising for more stable and long-lasting lithium batteries.

2. Experimental

2.1. Preparation of HKUST-1 (MOF) and alumina nanoparticles (ANP)

The $Cu_3(BTC)_2$ MOF was synthesized by dissolving trimesic acid (95%, Sigma-Aldrich) and copper(II) nitrate trihydrate (Puriss. p.a., 99–104%, Sigma-Aldrich) in 50 mL of ethanol (ACS reagent, Sigma-Aldrich) as described in detail else-

where.[37] The solution was refluxed under stirring (500 rpm) for 48 hours; then a blue solid precipitate was collected by vacuum filtration and washed with distilled water and ethanol. Finally, the solid was dried in a vacuum at 80 °C overnight and stored in an argon-filled glove box (MBraun, H_2O and O_2 <0.5 ppm) until further use. The HKUST-1 structure was confirmed by XRD analysis (Fig. S1a†).

The alumina nanoparticles (ANP) were synthesized as previously described.[38] A methanol (ACS Reagent, Sigma-Aldrich) solution of aluminum nitrate nonahydrate (ACS Reagent, ≥98%) was stirred at room temperature and mixed with ammonium hydroxide solution (NH_4OH, 28–30% NH_3 basis, Sigma-Aldrich) to reach a pH value of 11–12. The resulting suspension was centrifuged at 6000 rpm for 40 minutes, dried at 100 °C for 2 hours and calcined at 400 °C for 2 hours. The alumina structure was confirmed by XRD analysis (Fig. S1b†).

2.2. Preparation of the separators

Four different types of P(VDF-HFP) separators were prepared: (i) the bare P(VDF-HFP) (bare), (ii) HKUST-1-based one (single MOF), (iii) ANP-based one (single ANP), and, finally, (iv) the Janus membrane (Janus) assembled by the two single composite separators.

Single MOF and single ANP were prepared by mixing HKUST-1/P(VDF-HFP) and Al_2O_3/P(VDF-HFP) with weight ratios of 1 : 1 and 1 : 4, respectively, in zirconia jars using a planetary ball mill at 100 rpm for 2 cycles of 10 minutes. The investigated separators (bare, single MOF and single ANP) were obtained by dispersion in *N*-methylpyrrolidone (NMP, Sigma-Aldrich), where the solid loading of the slurry was fixed at 26 wt%. After stirring, the resulting mixture was cast on glass with a doctor blade to obtain a wet film of 100 μm thickness and finally slowly dried at room temperature. The resulting films (thickness in the range 35–50 μm) were cut into 2 cm^2 round disks and stored in an argon-filled dry box prior to use. The Janus separator was obtained by hot-pressing single MOF and single ANP at 50 °C for 30 seconds at 100 psi. In the case of MOFs, the resulting films (single MOF and Janus separators) were activated at 160 °C under high vacuum for 6 hours and finally stored in an argon-filled dry box to avoid moisture contamination (MBraun, H_2O and O_2 <0.5 ppm).

2.3. Cathode preparation and cell assembly

The cathode slurry was prepared by using 70 wt% of active material $LiNi_{0.5}Mn_{1.5}O_4$ (LNMO, MTI Corporation), 20 wt% conductive carbon (Timcal Imerys, ENSACO 350P), and 10 wt% binder (PVDF, Kynar). LNMO and carbon were initially mixed in zirconia jars using a planetary ball mill at 150 rpm for 10 min, followed by a 5 min break and another 10 min of milling in the reverse direction. Subsequently, the binder was added and mixed under the same conditions. The composite powder was dispersed in a solution of *N*-methylpyrrolidone (NMP) to obtain a slurry with solid loading of 26 wt% that was cast on a carbon-coated aluminium foil as a current collector. The cathode was finally dried under vacuum at 80 °C overnight and cut into 2 cm^2 round disks, finally stored in a dry glovebox. The mass loading of the active material was 3 mg cm^{-2}.

CR2032 coin cells were assembled in an argon-filled glovebox with LNMO as the cathode and Li metal as the anode (Sigma-Aldrich 99.9%, thickness 0.38 mm). The amount of liquid electrolyte was 120 μL for all the assembled cells. The electrochemical experiments were performed with a commercial electrolyte LP30 ($LiPF_6$ 1.0 M in EC : DMC 50 : 50 v/v, Sigma-Aldrich) enriched with 100 ppm of distilled water, in order to trigger the electrolyte degradation and better evaluate the scavenging capability of the composite separators. Karl Fischer titration was performed to determine the accurate water concentrations in the electrolyte. In the specific case of the asymmetric Janus separator, the alumina layer faced the cathode, whereas the MOF layer faced the lithium metal.

2.4. Characterization

X-ray powder diffraction (XRPD) patterns were collected by using a Bruker D8 Advance diffractometer with a monochromatic Cu source (Kα_1, λ = 1.5406 Å) operated at 40 kV and 40 mA. The Ar-filled sample holder was used in the case of moisture sensitive samples (*e.g.* MOF-based ones).

The XRD patterns of the cycled electrodes were measured by using a Bruker D8 Advance diffractometer with a monochromatic Mo source (Kα1, λ = 0.7107 Å) in Debye–Scherrer geometry operated at 50 kV and 45 mA.

Thermogravimetric analyses of the separators were performed by heating at 5 °C min^{-1} from room temperature up to 900 °C under an air atmosphere with a flow rate of 50 ml min^{-1} in a ceramic pan by means of an STA8000 analyser (PerkinElmer).

Static contact angle analyses were performed to study the wettability of the different separators by means of a KSV CAM200 instrument with the sessile drop method using LP30 electrolyte as liquid medium. Additionally, all the separators were subjected to uptake testing with the same commercial electrolyte (LP30) to assess any difference in electrolyte storage capacity. The membranes were soaked in liquid electrolyte, and after the surplus solution was absorbed with paper, the separators were weighed periodically. The absorption ratio was measured by the following formula, where m_0 and m_1 are the masses of the separator before and after electrolyte immersion, respectively:

$$\text{Electrolyte uptake} = \frac{m_1 - m_0}{m_0} \times 100\%$$

Superficial and cross-sectional SEM morphology analyses of the separators were made using an SNE-4500M Plus (SEC) scanning electron microscope operated at 20 kV. The samples were Au-coated before the analysis.

Dynamic mechanical analysis (DMA) measurements were performed on rectangular-shaped samples (7 mm × 5 mm) by means of a DMA 242 E Artemis (NETZSCH) equipped with a shear jaw for films. The breakage stress–strain test was carried out in tensile mode at 30 °C with an increment strain of 0.05% up to the film breakage. The frequency sweep tests were

carried out in the frequency range between 0.2 and 20 Hz at a constant strain of 0.05% at 30 °C, 50 °C and 70 °C.

Galvanostatic cycling with potential limitation (GCPL) was carried out on Li|LNMO-based cells by means of a Biologic BCS-810 battery tester in the voltage range between 3.0 V and 4.9 V (*vs.* Li^+/Li couple) at 1C (146 mA h g^{-1}). Two preliminary activation cycles at C/5 (I_d = 29.3 mA g^{-1}) and at C/2 (I_d = 73.5 mA g^{-1}), respectively, were performed to stabilize the interface. The capacity retentions of the investigated cells were calculated by considering the cycles carried out at 1C.

The potentiodynamic electrochemical impedance spectrometry (PEIS) spectra were collected on cells at room temperature by applying an AC voltage of 50 mV in the frequency range from 10 kHz to 0.1 Hz, both at the OCV (open circuit voltage) and every 50 cycles to investigate the evolution of the cell impedance upon cycling.

ICP-OES analyses were performed using a PerkinElmer Avio 220 max spectrometer, equipped with an AVIO glass cyclonic baffled spray chamber, a quartz torch and a dual backside-illuminated charge-coupled device (DBI-CCD) detector. After cycling, the cells were disassembled, the separator and the lithium metal anode were digested in a solution of HNO_3 for 4 days at room temperature and then analysed to quantify the dissolution rate of both TM ions. More specifically, the Ni and Mn quantifications were carried out in the axial mode at 231.604 and 257.610 nm as wavelengths, by an external standard calibration curve. ICP grade standards (1000 mg L^{-1}, Merck) were diluted to 0.3–0.6–2.0–5.0–9.0 mg L^{-1} and then acidified to a final concentration of 2% nitric acid (from ultrapure 65% HNO_3, Merck). The measurement conditions were as in the following: nebulization gas flow: 0.7 L min^{-1}; power RF: 1500 W; auxiliary gas flow: 0.2 L min^{-1}; peristaltic pump: 1 mL min^{-1}; and frequency: 500 Hz. The metal loss value is determined using the following formula, where mg_{Loss} is the mass of metal ion (Mn or Ni) detected in the analysed sample and mg_{Tot} is the total mass of metal ions in the pristine cathode:

$$\text{Metal loss}\,(\%) = \frac{mg_{Loss}}{mg_{Tot}} \times 100$$

Thermal abuse response of the cells with these different composite separators was studied by means of an accelerated rate calorimeter (ES-ARC, Thermal Hazard Technology, THT). Before the ARC test, the coin cells were completely charged (upper to 4.9 V) at a rate of C/16, and this voltage was maintained for 30 minutes. The accelerated rate calorimeter was operated in a heat-wait-search (HWS) mode with a sensitivity threshold detection limit of 0.02 °C min^{-1}. The tests were performed between 30–280 °C, with a step of 5 °C, and the system was allowed to equilibrate for 15 minutes. If the temperature change rate was detected to be over 0.02 °C min^{-1}, the calorimeter switched to exotherm mode, entering a self-heating domain. If the self-heating rate exceeded 1 °C min^{-1}, the thermal runaway was initiated.

3. Results and discussion

3.1. Design and characterization of a scavenging Janus separator

The introduction of bifunctional units to produce Janus separators is one of the emerging strategies to face detrimental phenomena such as unstable lithium electrodeposition, or to promote the ionic transport *via* enhanced surface charge and wettability. Several examples are reported in the literature on the optimization of Janus membranes, filled with different types of inorganic additives, that can guarantee performance improvements with respect to the Celgard™ benchmark.[35] Here, an asymmetric Janus separator is produced by assembling two different P(VDF-HFP)-based composite films, namely a nanosized Al_2O_3-based layer facing the cathode and a MOF-based layer facing the Li anode, as sketched in Fig. 1. Such films include fillers with scavenging capabilities towards detrimental small molecules (HF and H_2O) produced by degradation phenomena of the liquid electrolyte and triggered by water traces or temperature. The loading of both fillers (namely 1/1 w/w MOF/polymer and 1/4 w/w ANP/polymer) has been optimised after careful screening in order to find a proper balance between high scavenging efficiency and satisfactory mechanical properties. Such a configuration was designed to strategically locate the HF scavenger layer (the alumina nanoparticles) very close to the cathode to protect it from the TM dissolution. Meanwhile, the H_2O scavenger (MOF) was used as a molecular sieve and interfaced with the lithium anode to limit the detrimental impact of water on the metal surface chemistry.

The capability of the nanosized alumina as a scavenger of HF was recently discussed as a strategy to enhance the lifetime of both LNMO and NMC-based cells.[38] The trapping action exploits chemical bonding and the neutralization reaction to suppress cathode corrosion. The filler is also nanometric to enhance the surface available to the reaction with HF and to allow a homogeneous dispersion of the filler over the cathode. Chang *et al.* reported a fully MOF separator with in-built water

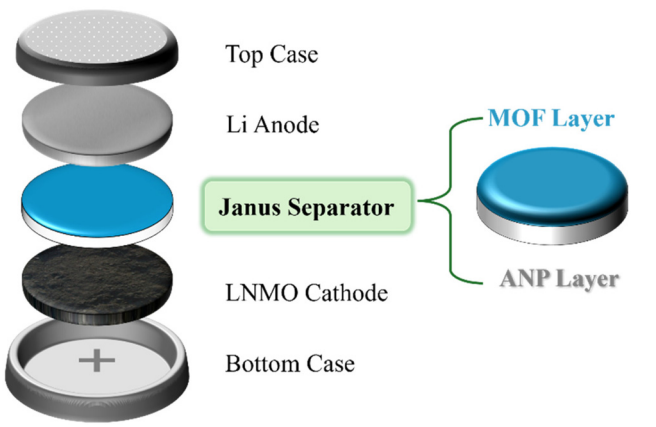

Fig. 1 Schematic representation of the cell configuration with the Janus separator.

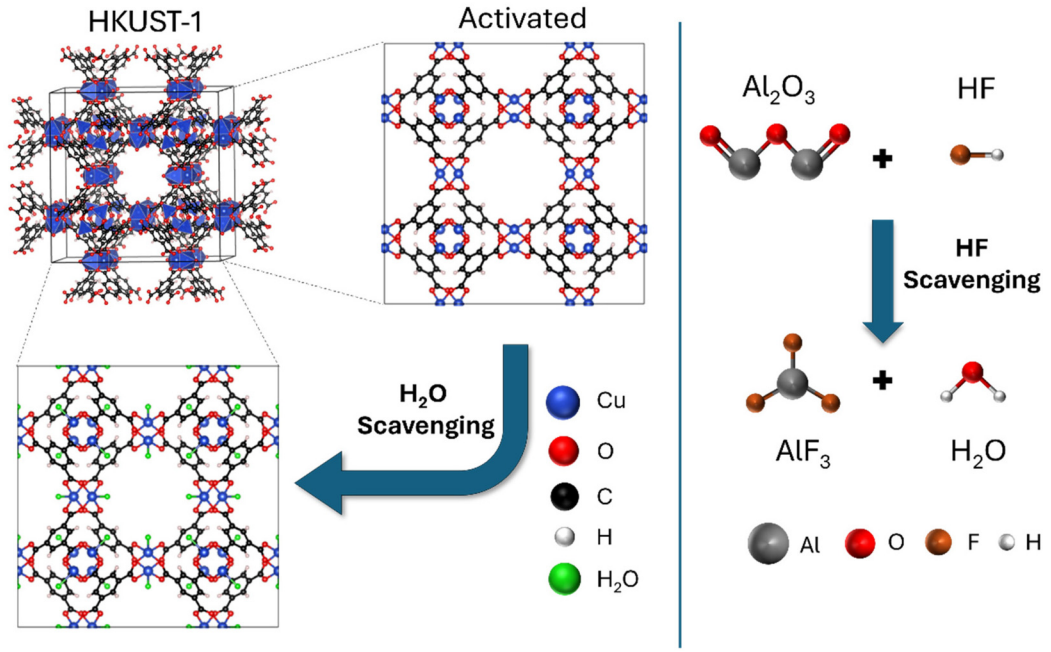

Fig. 2 Scavenging mechanism for H_2O and HF by HKUST-1 and Al_2O_3 nanoparticles, respectively.

scavenging activity paired with different cathode chemistries that suppressed the TM loss, allowing superior cycling stability if compared to the reference polymer separators.[33] The Janus membrane here proposed is designed to exploit the scavenging synergy of alumina and the MOF to simultaneously trap HF and water, even under drastic conditions (*e.g.* >100 ppm of water in the liquid electrolyte) while consequently improving both safety and lifespan of LNMO-based Li ion cells (Fig. 2).

The MOF here selected is $Cu_3(BTC)_2$ (namely HKUST-1) that can be used as a water scavenger due to its high capacity to reversibly exchange H_2O molecules. The typical microporous structure of the MOF further promotes its water trapping. Fig. S1† reports the XRD pattern of pristine HKUST-1 and nanosized Al_2O_3 that are in full accordance with the diffraction data reported in the literature for both the systems.[31,35] The XRD patterns of all the investigated separators, including the bare P(VDF-HFP) film for a sake of comparison, are included in Fig. S2†. These patterns show that the crystalline structure of the hosting polymer is not affected by the presence of a filler, making the typical γ-phase of the P(VDF-HFP) copolymer evident in all the separators, as proved by the presence of characteristic wide reflections peaked at 18.5 and 20.2°.[39,40]

As mentioned in the Experimental section, both the single MOF and Janus separators needed an activation step to confer scavenging capability owing to the unique HKUST-1 crystalline structure which promotes the reversible capture of the coordinated water molecules. This phenomenon is clearly proved by means of XRD analysis, evidencing the presence and the disappearance of the (111) peak (2θ = 5.86°) related to the coordination/de-coordination of the guest H_2O molecules on the metal site (Cu) in the MOF channels.[41] Indeed, the activated single MOF pattern (Fig. 3, violet line) shows the absence of the (111) signal that is instead evident in the deactivated pristine film (Fig. 3, cyan line). Moreover, the reversible water molecular exchange is easily indicated by the typical colour changes from cyan to violet blue under different humidity conditions (see inset Fig. 3), which is a proof of the altered coordination of the copper site. The scavenging capability was also confirmed by means of thermogravimetric analysis, as reported in Fig. S3†, comparing the thermograms of all the investigated separators. In the case of the single MOF sample, the loss of the coordination water of the cage structure takes place up to 200 °C, resulting in a weight loss of 4.5%, followed by the thermal decomposition of the MOF BTC ligands and of the polymer starting around 330 °C.[42]

Fig. 4 and Fig. S4† report the cross-sectional and top-view SEM images, respectively, of the separators evidencing clear morphological differences between the bare separator (Fig. 4a) and the composite ones (Fig. 4b–d). Specifically, the bare P(VDF-HFP) film exhibited a more compact matrix, whereas a network with sponge-like porosity was observed in the Janus separator and in the ANP- and MOF-based single layers. The porous network of the composite systems is likely the result of the incorporation of a great amount of filler in the polymer backbone (50 wt% and 20 wt% in the case of MOF and alumina, respectively), as frequently observed in the case of nanocomposite (gel) polymer electrolytes.[43–45] Such a morphological feature is beneficial in terms of higher liquid electrolyte uptake and improved lithium-ion transport across the membrane channels.[46]

As reported in Table 1, the thickness of the P(VDF-HFP)-based films is lower than 50 μm, while that of the Janus separator is about 90 μm, which is made by assembling the MOF- and ANP single layers.

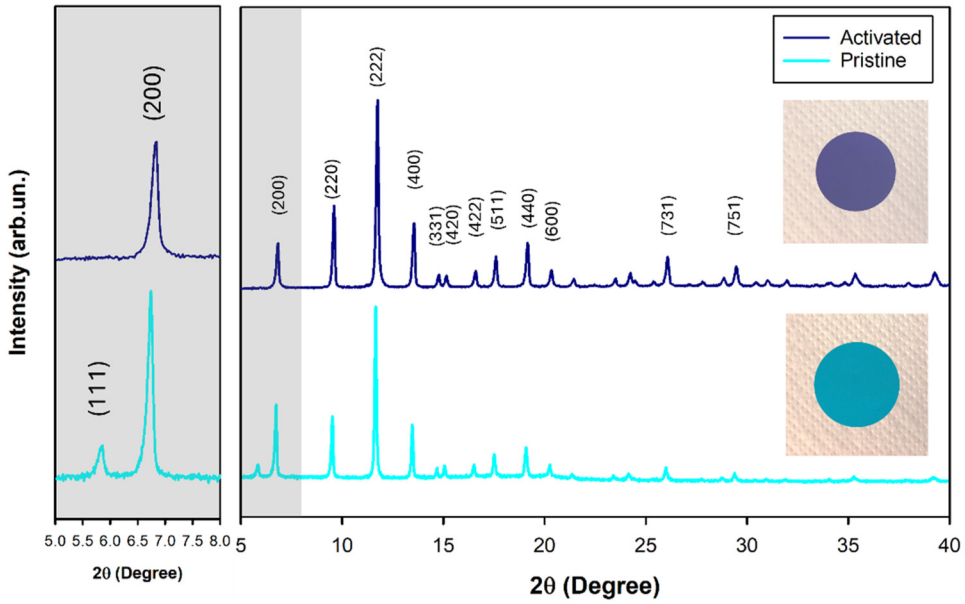

Fig. 3 XRD patterns of single MOF activated (violet line) and pristine (cyan line) films.

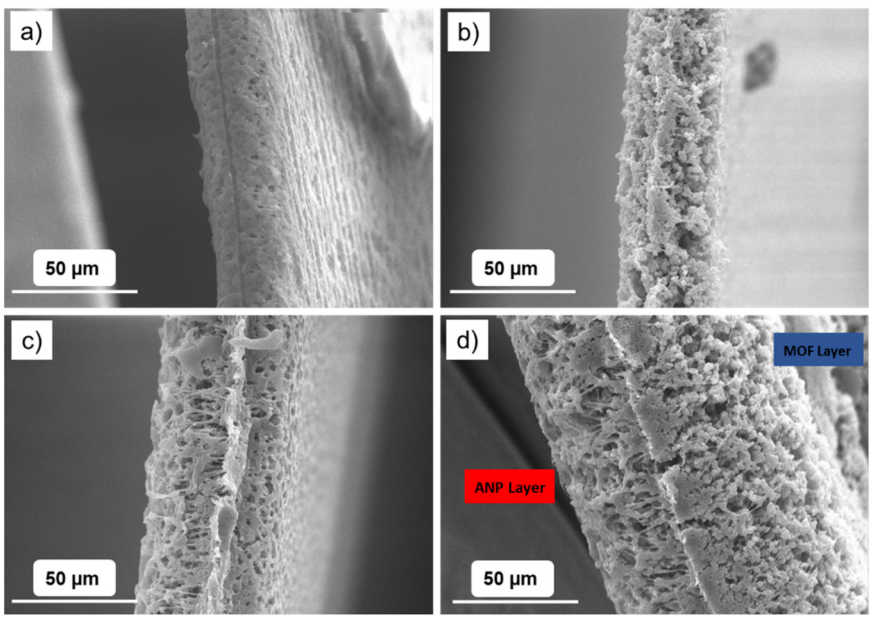

Fig. 4 Cross-section SEM images of (a) bare, (b) single MOF, (c) single ANP and (d) Janus separators.

In order to evaluate the effect of morphology on the separator affinity with the electrolyte, tests of liquid uptake were carried out by using the commercial LP30 solution, as reported in the Experimental section. The electrolyte uptake capacity of a separator is a crucial factor in improving the overall battery electrochemical performance, enhancing the ionic conductivity, and then decreasing the internal resistance.[47] As shown in Fig. 5, the plateau of the uptake ratio is achieved in less than 1 minute, by each separator, reaching values higher than 250 wt%. A smaller electrolyte uptake is obtained in the presence of HKUST-1 as filler in the MOF-based single layer, which suggests a less electrophilic behaviour exhibited by the organic framework with respect to the alumina nanoparticles, limiting to some extent the polymer swelling capability. However, the Janus separator shows an uptake of ~290% as the averaged value between the uptakes detected in both the single layers assembling the Janus membrane. Such a value is high enough to efficiently act as a separator; an uptake rate of about 300% is, in fact, usually achieved also by Celgard-like systems.[48] Similar trend is observed in the case of contact angle measure-

Table 1 Functional properties of the Janus separators compared to bare and single layers

		Bare	Single MOF	Single ANP	Janus
Thickness (μm)		35	50	45	90
Tensile strength (MPa)		1.30	0.20	0.50	0.35
Elongation (%)		4.8	1.8	3.4	2.9
E' (MPa) (1 Hz) (30 °C)		112.4	31.6	45.1	38.1
E'' (MPa) (1 Hz) (30 °C)		10.6	3.8	5.3	4.2
Capacity retention (%)		70	89	86	90
R_{CT} (Ω)	OCV	26.6	36.2	17.1	21.2
	After 100th cycles	89.5	139.7	79.5	14.7
	After 200th cycles	139.4	215	117.8	13.8

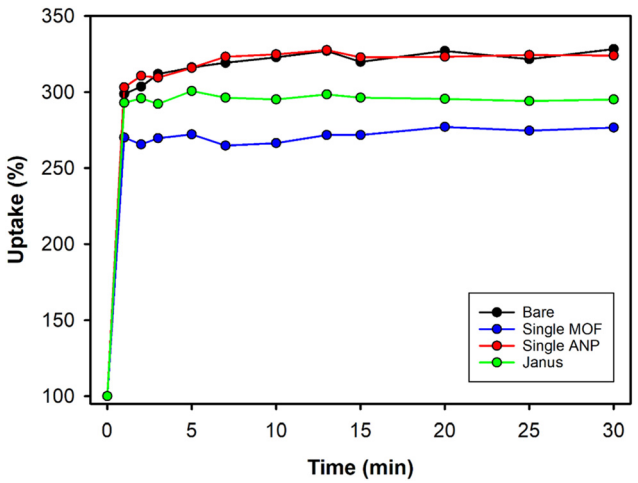

Fig. 5 Electrolyte uptake behaviour of the investigated separators with LP30.

ments reported in Fig. S5,† which demonstrates lower wettability for the MOF-based systems, both the MOF single layer (Fig. S5g–i†) and MOF-side of the Janus separator (Fig. S5j–l†), with respect to the ANP ones (Fig. S5d–f and Fig. S5m–o†).

Considering that the separator acts also as a physical barrier between the cathode and the anode, it should be capable of tolerating stress-inducing phenomena such as the assembly step during cell manufacturing and, at the microscopic level, the lithium dendrite nucleation and propagation. The addition of fillers into the polymer matrix can modify the mechanical properties of the resulting composite material.[14,49] DMA measurements were performed to evaluate the behaviour of the separator tensile strength and the viscoelastic moduli as a function of temperature and oscillation frequency. Fig. 6a reports the stress–strain curves of all the investigated separators as a function of the different fillers. The bare separator exhibits the highest tensile strength (1.3 MPa), while the elongation at break is 4.8%.

The composite membranes are less performing in terms of mechanical properties, especially in the case of MOF additive, maybe due to the high filler loading (20 wt% for single ANP and 50 wt% for single MOF), which can result in local particle aggregation (Fig. 6a and Table 1).[50] This result is in agreement with the literature, reporting that low to moderate loading of nanoparticles (<5%) improves the mechanical performance of polymer composites, while higher filler concentrations lead to a worsening of the system strength due to undesired effects such as nanoparticle agglomeration and/or inhomogeneous additive dispersion over the polymer matrix.[51–53] Despite the high amount of MOFs included in the Janus separator, the synergistic assembly of the two constituent layers (ANP and MOF-based ones) led to higher values of tensile strength (0.35 MPa) and elongation at break (2.9%) than those obtained for the single MOF-based separator.

The separator storage and loss moduli were studied as a function of frequency (0.2–20 Hz) at three different temperatures (30 °C, 50 °C and 70 °C), as reported in Fig. 6b and in ESI Fig. S6a and b.† As expected, by taking into consideration the stress–strain tests, E' and E'' values of the bare separator are higher than those measured for the composite systems in the entire explored temperature range. However, the mechanical strength is very good for all the investigated separators. For example, the storage modulus is more than one order of magnitude larger than the loss modulus, indicating that the separators have a solid-like behaviour. Moreover, both E' and E'' do not significantly change by increasing the frequency, which further confirms the stability of the materials, at least in the investigated frequency range.

3.2. Cycling performance of $LiNi_{0.5}Mn_{1.5}O_4$-based battery cells including the scavenging Janus separator under harsh conditions (water-enriched liquid electrolyte)

The scavenger capability of the Janus separator and its effect on the functional performance was explored through an *in situ* approach by means of electrochemical tests on cells including a liquid electrolyte enriched with 100 ppm of water at 25 °C and subsequent *post-mortem* analysis to quantify the TM dissolution rate and the eventual structural evolution of the spinel cathode. The Li|LMNO cell with the Janus separator was assembled with the LP30 electrolyte, and the resulting performances were compared with those obtained in the case of similar cells including bare, single MOF and single ANP separators. Fig. 7a shows the galvanostatic cycling at 1C over 200 cycles of the four assembled cells. The first four cycles were an activation step at a lower C-rate (C/5 and C/2) to guarantee the formation of a stable SEI. When cycled at a 1C current rate, the LMNO-based cell with a Janus separator delivers improved performance both in terms of

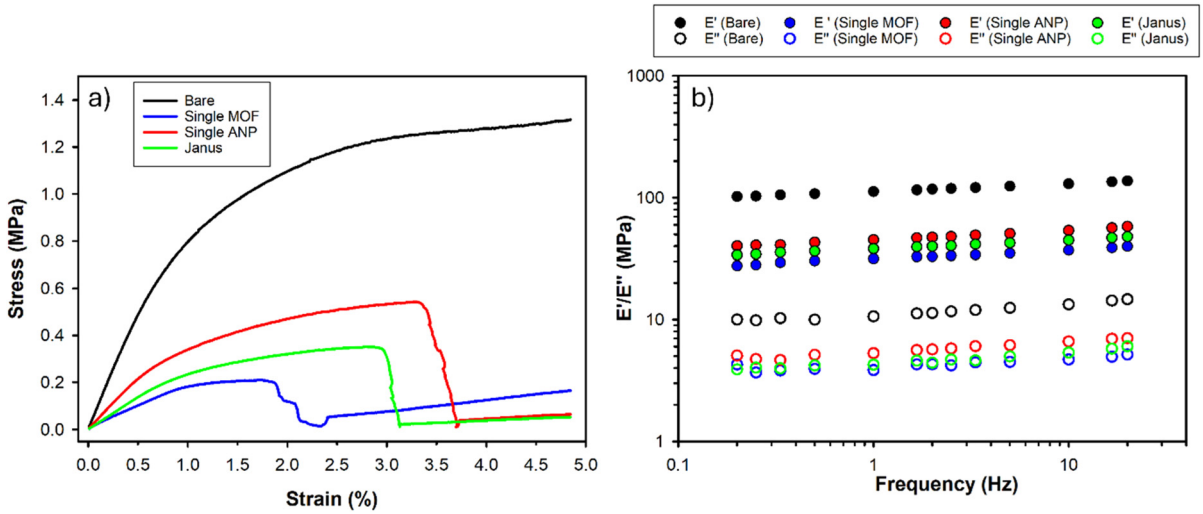

Fig. 6 (a) Stress–strain curves at 30 °C and (b) frequency-sweep tests at 30 °C for the investigated separators.

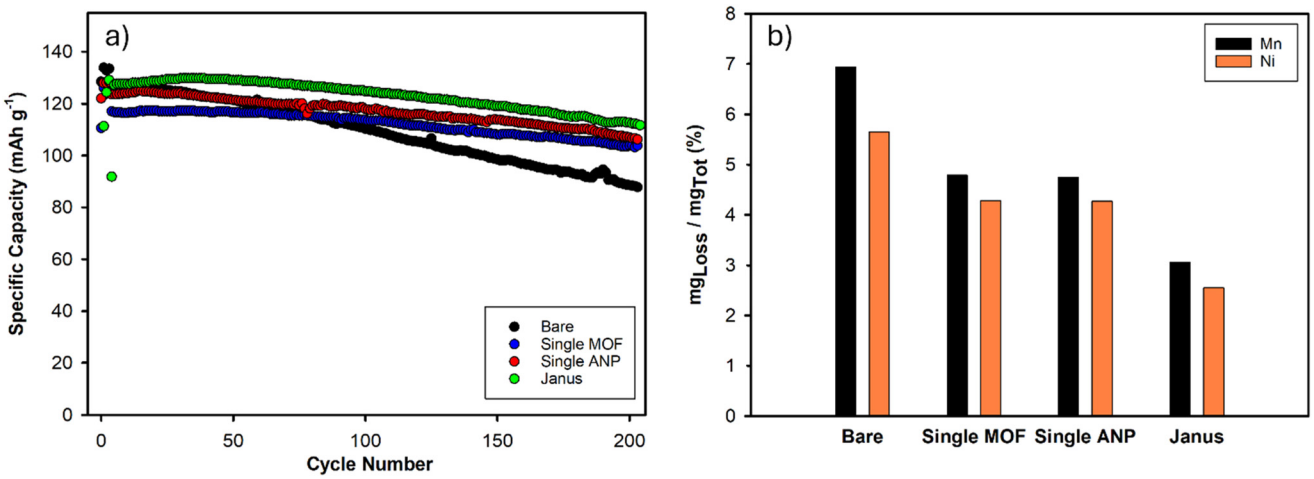

Fig. 7 (a) Discharge capacity at 1C of galvanostatically cycled LNMO|Li coin cells and (b) ICP quantification of metal loss percentages of the investigated separators with a water-enriched electrolyte (100 ppm of water), RSD (relative standard deviation) <1.5%.

discharge capacity and capacity retention, especially with respect to the bare system (pure P(VDF-HFP) without any filler). After 200 cycles, single MOF, single ANP and the Janus separator deliver discharge capacities of 104, 107 and 116 mA h g^{-1}, respectively, whereas the capacity of the bare-cell does not exceed 98 mA h g^{-1}. Moreover, the cell coupled with the Janus separator has an outstanding capacity retention of 90% after 200 cycles in contrast to the bare whose capacity decays much faster after only 80 cycles (Table 1). Comparable performances were obtained in the case of LNMO-cells including the Janus separator with anhydrous electrolyte (without any addition of water impurities) that deliver discharge capacity of about 135 mA h g^{-1} at 1C for the first 70 cycles with capacity retention of 89% at the end of the cycling test (see Fig. S7†). This is indirect experimental evidence of the scavenging capability of the Janus separator that can preserve good functional performance even in the presence of water traces.

The good performance exhibited by the Janus separator may be justified by the positive synergistic effect of the included scavenger fillers, namely HKUST-1 acting as water scavenger and nano-Al_2O_3 acting as a HF scavenger, that are able to hinder the electrolyte degradation process and to suppress the dissolution of TMs and ion crosstalk, induced by such two detrimental species.[33,54]

The exceptional improvement due to the separator scavenging capability was corroborated by the ICP analyses, carried out *post-mortem* on the disassembled separator and anode components, whose results are reported in Fig. 7b. The bare separator exhibits a significantly higher detrimental TM dissolution rate, with Mn and Ni losses of 7% and 5.5%, respectively. In contrast, cells containing scavenger agents (single MOF and single ANP) limit the Mn and Ni leaching at lower yields (4.5% and 4.0%, respectively) that are further reduced to 3% in the case of Mn and 2.5% for Ni

when the cell is cycled with the Janus membrane as the separator.

The beneficial effect of a multifunctional separator on the electrode–electrolyte interface was further confirmed by EIS measurements. The Nyquist plots collected for the cycled cells discussed in Fig. 7a, both at the OCV and upon cycling at the end of the 50th, 100th, 150th and 200th charge cycle at 4.9 V, are reported in Fig. S8.† All the spectra (both at the OCV and post-cycling) were best fitted by the equivalent circuit as depicted in Fig. S8e† to determine the cell interfacial resistance values, R_{CT}, listed in Table 1.[55] For what concerns bare, single MOF and single ANP, the spectra show a gradual increase of the charge transfer contribution upon cycling that may be ascribed to a modification of the electrode–electrolyte interface towards a less conductive layer in consequence of the degradation induced by the HF attack. This could mean that the presence of a single scavenger in the separator is insufficient to fully suppress the degradation phenomena taking place at the interface. In contrast, the Janus separator shows an overall constant interfacial resistance upon cycling with an R_{CT} value of 13.8 Ω after 200 cycles. This suggests the effective scavenging synergy of the Janus membrane to protect the electrode–electrolyte interface from the formation of insulating passivation layers or loss of electric contact caused by delamination or degradative phenomena.

To evaluate the structural stability of the LNMO cathode upon cycling in the presence of scavengers, *post-mortem* XRD and Rietveld analysis were performed on the cathode before cycling at the OCV and on the disassembled cathodes at the end of cycling. Fig. 8 compares the diffractograms of the LNMO cathodes cycled with the different separators. No significant differences are evident in the patterns ascribable to phase modification. However, the results of the Rietveld refinement analysis presented in Table S1† demonstrate a significant variation in the lattice parameter. Upon consideration of the electrode value at the OCV (a = 8.166(1) Å), in the case of the cell assembled with the bare separator, a decrease in this parameter was observed, with a value of a = 8.157(4) Å being recorded. This outcome indicates that a substantial structural change occurred, resulting in a reduction of the cell volume (at the OCV V = 544.5(2) Å^3 *vs.* bare V = 542.7(8) Å^3). The contraction of these parameters could be attributed to the high rate of leaching of TMs (Ni and Mn) from the lattice, which is observed in the absence of scavengers. In contrast, cells with functional scavengers exhibited essentially unaltered lattice parameter values. In the case of the cell with the Janus separator, the lattice parameter of the cathodic material was found to be 8.164(2) Å, indicating minimal variation in the material's structure, which agrees with the low leaching rates due to the presence of the scavengers.

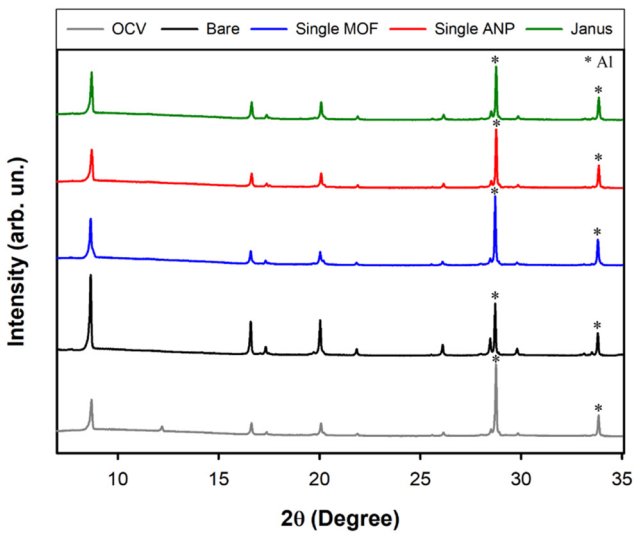

Fig. 8 XRD patterns collected for LNMO cathodes before cycling (OCV) and after 200 cycles with water-enriched LP30 for all the investigated separators.

3.3. Thermal abuse tests on $LiNi_{0.5}Mn_{1.5}O_4$-based battery cells under harsh conditions (water-enriched liquid electrolyte)

Thermal abuse analyses were carried out by ES-ARC, which can provide an adiabatic environment with accurate control. The tests were performed on coin cells with all the investigated separators: bare, single MOF, single ANP and Janus. This analysis simulates the thermal behaviour in an exothermic process where the generated heat is not quickly dissipated by the battery case, potentially leading to a thermal runaway with possible hazardous repercussions. In this experiment, several key parameters were identified: the onset temperature of the exothermal reaction (T_{EXO}), the onset of the thermal runaway (T_{OTR}) and the maximum self-heating rate (SHR_{MAX}).[56,57]

Fig. 9 shows the temperature *vs.* time curves of the LNMO water-enriched cells, and Table 2 reports the corresponding thermal parameters. After several cycles of the heat-wait-search process, all the cells reached the onset of the exothermal reaction, which is ascribable to the solid electrolyte interface (SEI) decomposition. This phenomenon triggers a chain reaction (*e.g.* anode, cathode, and electrolyte decomposition), generating more heat until the self-heating causes thermal runaway.[58] The cell with a bare separator exhibited a lower T_{EXO} (161.2 °C) and a significantly higher self-heating rate (1.125 °C min^{-1}) compared to the other cells. This reflected the thermal instability of the cell, including separators without scavengers that were not capable of buffering the detrimental processes induced by the traces of water present in the electrolyte, resulting in thermal runaway (T_{OTR} 182.0 °C). The presence of scavenging units in the cell, especially in synergistic assets as for the Janus system, seemed to give remarkable benefits also from a thermal point of view in relation to the HF-induced corrosive action. Indeed, the self-heating rates of all the cells, including scavenging separators, were smaller than that observed in the case of the bare P(VDF-HFP) film, especially in the presence of the Janus membrane, where an exceptionally low SHR of just 0.323 °C min^{-1} was measured (Table 2). Moreover, the Janus separator-based cell was more resistant towards the thermal abuse, with an onset temperature (T_{EXO}

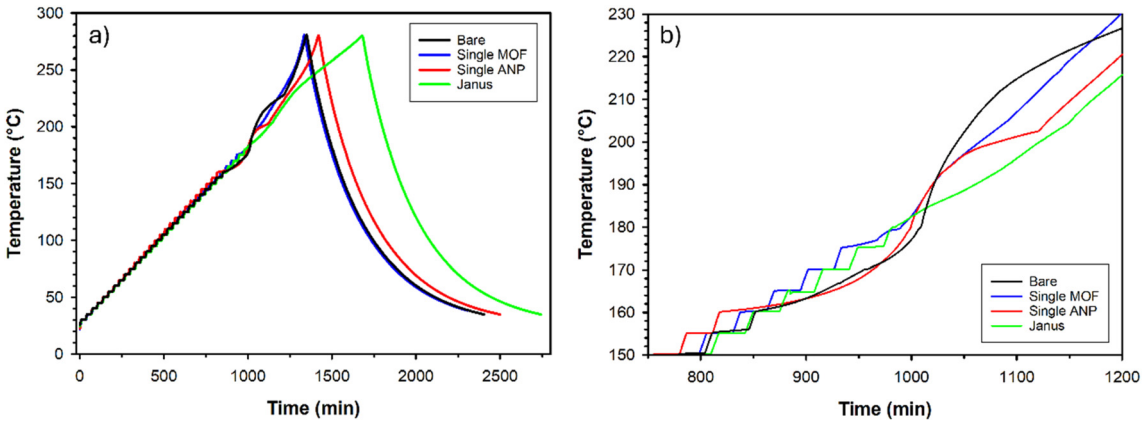

Fig. 9 (a) Thermal abuse test on LNMO coin cells including a 100 ppm water-enriched liquid electrolyte; (b) magnification of the onset of the exothermal phenomena.

Table 2 Thermal parameters of the accelerated rate calorimetry (ARC) test on the LNMO coin cells with the investigated separators

	Bare	Single MOF	Single ANP	Janus
T_{EXO} (°C)	161.2	176	160.7	182.2
T_{OTR} (°C)	182.0	—	—	—
t_{MAX} (min)	1346	1334	1418	1680
SHR_{MAX} (°C/ min^{-1})	1.125	0.722	0.912	0.323

182.2 °C) higher than that detected for the bare one (T_{EXO} 161.2 °C).

4. Conclusions

A novel bifunctional Janus membrane was investigated as a scavenging separator for high-voltage lithium-ion batteries. The separator was realized by assembling two P(VDF-HFP)-based composite films including different scavenging agents: (i) one side, faced with the Li anode, was filled with a metal–organic framework, namely HKUST-1, acting as a sieve to reversibly trap water molecules in its channels through coordination at the Cu-metallic center; (ii) the second side, faced with the LNMO cathode, included alumina nanoparticles capable of neutralizing even small traces of hydrofluoric acid.

The introduction of the scavengers into the separator resulted in an effective and synergetic approach for simultaneously mitigating the detrimental effects of small molecules, such as H_2O and HF, generated by the lithium salt degradation triggered by the presence of humidity and other impurities and/or a temperature increase. Pairing the Janus separator with the $LiNi_{0.5}Mn_{1.5}O_4$-based cathode in the presence of a water-enriched electrolyte, we proved significantly enhanced cycling stability, with capacity loss <12% after 200 cycles, at least three times lower than the capacity fading observed in the case of cells including the bare P(VDF-HFP) separator. The superior functional performances of the scavenging Janus membrane are reasonably related to the observed remarkable reduction of the dissolution of TMs from the cathode, limiting the leached ion crosstalk through the electrolyte. This also resulted in very high resistance towards thermal runaway processes, as demonstrated by overheating tests carried out on coin cells with heavily water-contaminated electrolytes. The proposed strategy highlights how lithium-ion batteries can significantly benefit from the use of multifunctional scavengers to improve the cell quality, reliability, lifetime, and safety.

Data availability

All data supporting the findings of this study are included in this article and its ESI.†

Conflicts of interest

There are no conflicts to declare.

Acknowledgements

The authors are grateful for the support of the MUR-PRIN "Healib" project funded by the European Union Next-GenerationEU. This study was carried out within the MOST–Sustainable Mobility Center and received funding from the European Union Next-GenerationEU (PIANO NAZIONALE DI RIPRESA E RESILIENZA (PNRR)–MISSIONE 4 COMPONENTE 2, INVESTIMENTO 1.4–D.D. 1033 17/06/2022, CN00000023). This manuscript reflects only the authors' views and opinions; neither the European Union nor the European Commission can be considered responsible for them.

References

1 M. Li, J. Lu, Z. Chen and K. Amine, 30 Years of Lithium-Ion Batteries, *Adv. Mater.*, 2018, **30**(33), DOI: **10.1002/adma.201800561**.

2 I. Burch and J. Gilchrist, *Survey of Global Activity to Phase Out Internal Combustion Engine Vehicles*, 2018. https://www.theclimatecenter.org.

3 J. Liu, M. Yue, S. Wang, Y. Zhao and J. Zhang, A Review of Performance Attenuation and Mitigation Strategies of Lithium-Ion Batteries, *Adv. Funct. Mater.*, 2022, **32**(8), DOI: 10.1002/adfm.202107769.

4 L. Mezzomo, C. Ferrara, G. Brugnetti, D. Callegari, E. Quartarone, P. Mustarelli and R. Ruffo, Exploiting Self-Healing in Lithium Batteries: Strategies for Next-Generation Energy Storage Devices, *Adv. Energy Mater.*, 2020, **10**(46), DOI: 10.1002/aenm.202002815.

5 J. Han, K. Kim, Y. Lee and N. Choi, Scavenging Materials to Stabilize $LiPF_6$-Containing Carbonate-Based Electrolytes for Li-Ion Batteries, *Adv. Mater.*, 2019, **31**(20), DOI: 10.1002/adma.201804822.

6 R. Narayan, C. Laberty-Robert, J. Pelta, J. Tarascon and R. Dominko, Self-Healing: An Emerging Technology for Next-Generation Smart Batteries, *Adv. Energy Mater.*, 2022, **12**(17), DOI: 10.1002/aenm.202102652.

7 X. Han, L. Lu, Y. Zheng, X. Feng, Z. Li, J. Li and M. Ouyang, A Review on the Key Issues of the Lithium Ion Battery Degradation among the Whole Life Cycle, *eTransportation*, 2019, **1**, 100005, DOI: 10.1016/j.etran.2019.100005.

8 N. P. W. Pieczonka, Z. Liu, P. Lu, K. L. Olson, J. Moote, B. R. Powell and J.-H. Kim, Understanding Transition-Metal Dissolution Behavior in $LiNi_{0.5}Mn_{1.5}O_4$ High-Voltage Spinel for Lithium Ion Batteries, *J. Phys. Chem. C*, 2013, **117**(31), 15947–15957, DOI: 10.1021/jp405158m.

9 C. Zhan, T. Wu, J. Lu and K. Amine, Dissolution, Migration, and Deposition of Transition Metal Ions in Li-Ion Batteries Exemplified by Mn-Based Cathodes – a Critical Review, *Energy Environ. Sci.*, 2018, **11**(2), 243–257, DOI: 10.1039/C7EE03122J.

10 W. Li, U.-H. Kim, A. Dolocan, Y.-K. Sun and A. Manthiram, Formation and Inhibition of Metallic Lithium Microstructures in Lithium Batteries Driven by Chemical Crossover, *ACS Nano*, 2017, **11**(6), 5853–5863, DOI: 10.1021/acsnano.7b01494.

11 J. Hong, H.-D. Lim, M. Lee, S.-W. Kim, H. Kim, S.-T. Oh, G.-C. Chung and K. Kang, Critical Role of Oxygen Evolved from Layered Li–Excess Metal Oxides in Lithium Rechargeable Batteries, *Chem. Mater.*, 2012, **24**(14), 2692–2697, DOI: 10.1021/cm3005634.

12 S. S. Zhang, A Review on Electrolyte Additives for Lithium-Ion Batteries, *J. Power Sources*, 2006, **162**(2), 1379–1394, DOI: 10.1016/j.jpowsour.2006.07.074.

13 Z. Zou, H. Xu, H. Zhang, Y. Tang and G. Cui, Electrolyte Therapy for Improving the Performance of $LiNi_{0.5}Mn_{1.5}O_4$ Cathodes Assembled Lithium–Ion Batteries, *ACS Appl. Mater. Interfaces*, 2020, **12**(19), 21368–21385, DOI: 10.1021/acsami.0c02516.

14 S. T. Muntha, A. Kausar and M. Siddiq, A Review Featuring Fabrication, Properties, and Application of Polymeric Mixed Matrix Membrane Reinforced with Different Fillers, *Polym.-Plast. Technol. Eng.*, 2017, **56**(18), 2043–2064, DOI: 10.1080/03602559.2017.1298801.

15 P. Li, Y. Wang, Z. Liu and X. Hu, Acid-Scavenging Separators Promise Long-Term Cycling Stability of Lithium-Ion Batteries, *Mater. Chem. Front.*, 2023, **7**(24), 6318–6344, DOI: 10.1039/D3QM00709J.

16 A. Banerjee, B. Ziv, Y. Shilina, S. Luski, D. Aurbach and I. C. Halalay, Acid-Scavenging Separators: A Novel Route for Improving Li-Ion Batteries' Durability, *ACS Energy Lett.*, 2017, **2**(10), 2388–2393, DOI: 10.1021/acsenergylett.7b00763.

17 S. Yan, X. Sun, Y. Zhang, S. Fu, Y. Lang, L. Wang and G. Liang, From Coating to Doping: Effect of Post-Annealing Temperature on the Alumina Coating of $LiNi_{0.5}Mn_{1.5}O_4$ Cathode Material, *J. Solid State Chem.*, 2022, **306**, 122765, DOI: 10.1016/j.jssc.2021.122765.

18 J. Soon, T. J. Lee, H. Kim, J. Jung, J. H. Ryu and S. M. Oh, Copper Oxide as a Hydrogen Fluoride Scavenger for High-Voltage $LiNi_{0.5}Mn_{1.5}O_4$ Positive Electrode, *J. Electrochem. Soc.*, 2017, **164**(12), A2677–A2682, DOI: 10.1149/2.1641712jes.

19 J.-S. Kim, C. S. Johnson, J. T. Vaughey, S. A. Hackney, K. A. Walz, W. A. Zeltner, M. A. Anderson and M. M. Thackeray, The Electrochemical Stability of Spinel Electrodes Coated with ZrO_2, Al_2O_3, and SiO_2 from Colloidal Suspensions, *J. Electrochem. Soc.*, 2004, **151**(10), A1755, DOI: 10.1149/1.1793713.

20 Y. Sun, Electrochemical Performance of Nano-Sized ZnO-Coated $LiNi_{0.5}Mn_{1.5}O_4$ Spinel as 5 V Materials at Elevated Temperatures, *Electrochem. Commun.*, 2002, **4**(4), 344–348, DOI: 10.1016/S1388-2481(02)00277-1.

21 Z. Qiu, S. Yuan, Z. Wang, L. Shi, J. H. Jo, S.-T. Myung and J. Zhu, Construction of Silica-Oxygen-Borate Hybrid Networks on Al_2O_3-Coated Polyethylene Separators Realizing Multifunction for High-Performance Lithium Ion Batteries, *J. Power Sources*, 2020, **472**, 228445, DOI: 10.1016/j.jpowsour.2020.228445.

22 Y. Han, P. Qi, J. Zhou, X. Feng, S. Li, X. Fu, J. Zhao, D. Yu and B. Wang, Metal–Organic Frameworks (MOFs) as Sandwich Coating Cushion for Silicon Anode in Lithium Ion Batteries, *ACS Appl. Mater. Interfaces*, 2015, **7**(48), 26608–26613, DOI: 10.1021/acsami.5b08109.

23 Z. A. Qureshi, H. A. Tariq, R. A. Shakoor, R. Kahraman and S. AlQaradawi, Impact of Coatings on the Electrochemical Performance of $LiNi_{0.5}Mn_{1.5}O_4$ Cathode Materials: A Focused Review, *Ceram. Int.*, 2022, **48**(6), 7374–7392, DOI: 10.1016/j.ceramint.2021.12.118.

24 J. C. Barbosa, R. Gonçalves, C. M. Costa, V. de Zea Bermudez, A. Fidalgo-Marijuan, Q. Zhang and S. Lanceros-Méndez, Metal–Organic Frameworks and Zeolite Materials as Active Fillers for Lithium-Ion Battery Solid Polymer Electrolytes, *Mater. Adv.*, 2021, **2**(12), 3790–3805, DOI: 10.1039/D1MA00244A.

25 J. Feng, L. Wang, Y. Chen, P. Wang, H. Zhang and X. He, PEO Based Polymer-Ceramic Hybrid Solid Electrolytes: A Review, *Nano Convergence*, 2021, **8**(1), 2, DOI: 10.1186/s40580-020-00252-5.

26 M. Farina, B. B. Duff, C. Tealdi, A. Pugliese, F. Blanc and E. Quartarone, Li^+ Dynamics of Liquid Electrolytes

Nanoconfined in Metal–Organic Frameworks, *ACS Appl. Mater. Interfaces*, 2021, **13**(45), 53986–53995, DOI: **10.1021/acsami.1c16214**.

27 Y. Ren, K. Chen, R. Chen, T. Liu, Y. Zhang and C. Nan, Oxide Electrolytes for Lithium Batteries, *J. Am. Ceram. Soc.*, 2015, **98**(12), 3603–3623, DOI: **10.1111/jace.13844**.

28 S. Li, S. Zhang, L. Shen, Q. Liu, J. Ma, W. Lv, Y. He and Q. Yang, Progress and Perspective of Ceramic/Polymer Composite Solid Electrolytes for Lithium Batteries, *Adv. Sci.*, 2020, **7**(5), DOI: **10.1002/advs.201903088**.

29 H. Furukawa, K. E. Cordova, M. O'Keeffe and O. M. Yaghi, The Chemistry and Applications of Metal-Organic Frameworks, *Science*, 2013, **341**(6149), DOI: **10.1126/science.1230444**.

30 J.-R. Li, J. Sculley and H.-C. Zhou, Metal–Organic Frameworks for Separations, *Chem. Rev.*, 2012, **112**(2), 869–932, DOI: **10.1021/cr200190s**.

31 S. S.-Y. Chui, S. M.-F. Lo, J. P. H. Charmant, A. G. Orpen and I. D. Williams, A Chemically Functionalizable Nanoporous Material $[Cu_3(TMA)_2(H_2O)_3]_n$, *Science*, 1999, **283**(5405), 1148–1150, DOI: **10.1126/science.283.5405.1148**.

32 P. Küsgens, M. Rose, I. Senkovska, H. Fröde, A. Henschel, S. Siegle and S. Kaskel, Characterization of Metal-Organic Frameworks by Water Adsorption, *Microporous Mesoporous Mater.*, 2009, **120**(3), 325–330, DOI: **10.1016/j.micromeso.2008.11.020**.

33 Z. Chang, Y. Qiao, H. Deng, H. Yang, P. He and H. Zhou, A Stable High-Voltage Lithium-Ion Battery Realized by an in-Built Water Scavenger, *Energy Environ. Sci.*, 2020, **13**(4), 1197–1204, DOI: **10.1039/D0EE00060D**.

34 D. Chan, Y. Liu, Y. Fan, H. Wang, S. Chen, T. Hao, H. Li, Z. Bai, H. Shao, G. Xing, Y. Zhang and Y. Tang, Functional Janus Membranes: Promising Platform for Advanced Lithium Batteries and Beyond, *Energy Environ. Mater.*, 2023, **6**(5), DOI: **10.1002/eem2.12451**.

35 D. Callegari, S. Davino, M. Parmigiani, M. Medina-Llamas, L. Malavasi and E. Quartarone, Multifunctional Janus Separators for Safer and Dendrite-Free Lithium-Metal Batteries, *Batteries Supercaps*, 2023, **6**(12), DOI: **10.1002/batt.202300431**.

36 C. Zhang, X. Lan, Q. Liu, L. Yu, Y. Li and X. Hu, Bi-Functional Janus All-Nanomat Separators for Acid Scavenging and Manganese Ions Trapping in LiMn2O4 Lithium-Ion Batteries, *Mater. Today Phys.*, 2022, **24**, 100676, DOI: **10.1016/j.mtphys.2022.100676**.

37 J. Kim, S.-H. Kim, S.-T. Yang and W.-S. Ahn, Bench-Scale Preparation of $Cu_3(BTC)_2$ by Ethanol Reflux: Synthesis Optimization and Adsorption/Catalytic Applications, *Microporous Mesoporous Mater.*, 2012, **161**, 48–55, DOI: **10.1016/j.micromeso.2012.05.021**.

38 D. Callegari, M. Canini, S. Davino, M. Coduri, P. Mustarelli and E. Quartarone, Chitosan-Decorated Alumina Hybrid Nanoparticles as Smart Scavengers of HF and Dissolved Transition Metals in Lithium-Ion Batteries, *Adv. Funct. Mater.*, 2024, DOI: **10.1002/adfm.202406315**.

39 X. Cai, T. Lei, D. Sun and L. Lin, A Critical Analysis of the α, β and γ Phases in Poly(Vinylidene Fluoride) Using FTIR, *RSC Adv.*, 2017, **7**(25), 15382–15389, DOI: **10.1039/C7RA01267E**.

40 P. Martins, A. C. Lopes and S. Lanceros-Mendez, Electroactive Phases of Poly(Vinylidene Fluoride): Determination, Processing and Applications, *Prog. Polym. Sci.*, 2014, **39**(4), 683–706, DOI: **10.1016/j.progpolymsci.2013.07.006**.

41 L. Shen, H. B. Wu, F. Liu, J. L. Brosmer, G. Shen, X. Wang, J. I. Zink, Q. Xiao, M. Cai, G. Wang, Y. Lu and B. Dunn, Creating Lithium-Ion Electrolytes with Biomimetic Ionic Channels in Metal–Organic Frameworks, *Adv. Mater.*, 2018, **30**(23), DOI: **10.1002/adma.201707476**.

42 J. de Haro, A. Benítez, Á. Caballero and J. Morales, Revisiting the HKUST-1/S Composite as an Electrode for Li-S Batteries: Inherent Problems That Hinder Its Performance, *Eur. J. Inorg. Chem.*, 2021, **2021**(2), 177–185, DOI: **10.1002/ejic.202000837**.

43 V. P. Hoang Huy, S. So and J. Hur, Inorganic Fillers in Composite Gel Polymer Electrolytes for High-Performance Lithium and Non-Lithium Polymer Batteries, *Nanomaterials*, 2021, **11**(3), 614, DOI: **10.3390/nano11030614**.

44 N. Yadav, K. Mishra and S. Hashmi, Nanofiller-Incorporated Porous Polymer Electrolyte for Electrochemical Energy Storage Devices, *High Perform. Polym.*, 2018, **30**(8), 957–970, DOI: **10.1177/0954008318774392**.

45 G. Kanimozhi, N. Naresh, H. Kumar and N. Satyanarayana, Review on the Recent Progress in the Nanocomposite Polymer Electrolytes on the Performance of Lithium-ion Batteries, *Int. J. Energy Res.*, 2022, **46**(6), 7137–7174, DOI: **10.1002/er.7740**.

46 X. Hu, Q. Liu, K. Lin, C. Han and B. Li, The Rise of Metal–Organic Frameworks for Electrolyte Applications, *J. Mater. Chem. A*, 2021, **9**(37), 20837–20856, DOI: **10.1039/D1TA05201B**.

47 S. C. Mun and J. H. Won, Manufacturing Processes of Microporous Polyolefin Separators for Lithium-Ion Batteries and Correlations between Mechanical and Physical Properties, *Crystals*, 2021, **11**(9), 1013, DOI: **10.3390/cryst11091013**.

48 P. Cattaneo, D. Callegari, D. Merli, C. Tealdi, D. Vadivel, C. Milanese, V. Kapelyushko, F. D'Aprile and E. Quartarone, Sorting, Characterization, Environmentally Friendly Recycling, and Reuse of Components from End-of-Life 18650 Li Ion Batteries, *Adv. Sustainable Syst.*, 2023, **7**(9), DOI: **10.1002/adsu.202300161**.

49 F. Zheng, C. Li, Z. Li, X. Cao, H. Luo, J. Liang, X. Zhao and J. Kong, Advanced Composite Solid Electrolytes for Lithium Batteries: Filler Dimensional Design and Ion Path Optimization, *Small*, 2023, **19**(21), DOI: **10.1002/smll.202206355**.

50 H. S. Varol, F. Meng, B. Hosseinkhani, C. Malm, D. Bonn, M. Bonn, A. Zaccone and S. H. Parekh, Nanoparticle

Amount, and Not Size, Determines Chain Alignment and Nonlinear Hardening in Polymer Nanocomposites, *Proc. Natl. Acad. Sci. U. S. A.*, 2017, **114**(16), DOI: **10.1073/pnas.1617069114**.

51 V. G. Nguyen, H. Thai, D. H. Mai, H. T. Tran, D. L. Tran and M. T. Vu, Effect of Titanium Dioxide on the Properties of Polyethylene/TiO_2 Nanocomposites, *Composites, Part B*, 2013, **45**(1), 1192–1198, DOI: **10.1016/j.compositesb.2012.09.058**.

52 M. S. Goyat and P. K. Ghosh, Impact of Ultrasonic Assisted Triangular Lattice like Arranged Dispersion of Nanoparticles on Physical and Mechanical Properties of Epoxy-TiO_2 Nanocomposites, *Ultrason. Sonochem.*, 2018, **42**, 141–154, DOI: **10.1016/j.ultsonch.2017.11.019**.

53 H. Salehian and S. A. Jenabali Jahromi, Effect, of Titanium Dioxide Nanoparticles on Mechanical Properties of Vinyl Ester-Based Nanocomposites, *J. Compos. Mater.*, 2015, **49**(19), 2365–2373, DOI: **10.1177/0021998314546140**.

54 Y. Tesfamhret, R. Younesi and E. J. Berg, Influence of Al_2O_3 Coatings on HF Induced Transition Metal Dissolution from Lithium-Ion Cathodes, *J. Electrochem. Soc.*, 2022, **169**(1), 010530, DOI: **10.1149/1945-7111/ac4ab1**.

55 D. Aurbach, B. Markovsky, Y. Talyossef, G. Salitra, H.-J. Kim and S. Choi, Studies of Cycling Behavior, Ageing, and Interfacial Reactions of $LiNi_{0.5}Mn_{1.5}O_4$ and Carbon Electrodes for Lithium-Ion 5-V Cells, *J. Power Sources*, 2006, **162**(2), 780–789, DOI: **10.1016/j.jpowsour.2005.07.009**.

56 A. Börger, J. Mertens and H. Wenzl, Thermal Runaway and Thermal Runaway Propagation in Batteries: What Do We Talk About?, *J. Energy Storage*, 2019, **24**, 100649, DOI: **10.1016/j.est.2019.01.012**.

57 X. Feng, S. Zheng, D. Ren, X. He, L. Wang, H. Cui, X. Liu, C. Jin, F. Zhang, C. Xu, H. Hsu, S. Gao, T. Chen, Y. Li, T. Wang, H. Wang, M. Li and M. Ouyang, Investigating the Thermal Runaway Mechanisms of Lithium-Ion Batteries Based on Thermal Analysis Database, *Appl. Energy*, 2019, **246**, 53–64, DOI: **10.1016/j.apenergy.2019.04.009**.

58 X. Feng, M. Ouyang, X. Liu, L. Lu, Y. Xia and X. He, Thermal Runaway Mechanism of Lithium Ion Battery for Electric Vehicles: A Review, *Energy Storage Mater.*, 2018, **10**, 246–267, DOI: **10.1016/j.ensm.2017.05.013**.